

# **Three Dimensional Image Based Meshing and Computational Analysis of Fluid Flow in Various Porous Media**

**For Group Project:**

## **Investigating Stormwater Filters and Bioretention Systems**

A Study on the *Hydro Filterra<sup>(TM)</sup>* System Manufactured by *Hydro International (UK)*



**Individual Report – I2**

**2012**

**Alastair Begley  
580004470  
032759**

Supervisor: Dr Gavin Tabor

# Abstract

A micro scale computational study investigating the flow of water through porous media used in the *Hydro Filterra™* Bioretention system designed by *Hydro International (UK)*. A model is constructed accurately representing the pore geometry using Image Based Meshing (IBM) on data obtained from micro CT scans of the filter media. The fluid flow through this model will then be analysed using Computational Fluid Dynamics (CFD) in order to solve the Navier-Stokes equations. This report will investigate the modelling techniques required to use IBM on filter media and then how to generate a CFD model. The knowledge gained from this process will then be used to compare the results of different filter media samples, one sourced directly from *Hydro International (UK)* and one which was sampled from an active *Hydro Filterra™* site. These results will then be compared to experimental data obtained by scaling the model generated from image based meshing and created using additive layer manufacturing in order validate the computational model.

## Keywords

Image Based Meshing, Porous Media, Computational Fluid Dynamics, Filter Media, Packed Bed

# Acknowledgements

Thanks must be given to:

- Simpleware Ltd. for providing a license for the use of their software, *ScanIP*, for the duration of this project which enable image based meshing to be used and also supplying their beta version of *ScanIP* to enable direct export to an *OpenFOAM* mesh.
- Dr Gavin Tabor whose help with *OpenFOAM* has been invaluable.

# Contents

<b>1</b>	<b>Introduction</b>	<b>1</b>
1.1	Stormwater Management . . . . .	1
1.2	Bioretention Systems . . . . .	1
1.2.1	<i>Hydro Filterra™</i> System . . . . .	2
1.3	Water Flow Analysis . . . . .	2
1.3.1	Micro Scale Computational Analysis . . . . .	3
1.4	Project Aims & Deliverables . . . . .	3
1.4.1	Group Aims & Deliverables . . . . .	3
1.4.2	Individual Aims & Deliverables . . . . .	3
<b>2</b>	<b>Management</b>	<b>5</b>
2.1	Individual Management . . . . .	5
2.2	Group Management . . . . .	5
<b>3</b>	<b>Review</b>	<b>8</b>
3.1	Packed Beds . . . . .	8
3.2	Image Based Meshing . . . . .	9
3.3	Computational Fluid Dynamics . . . . .	11
3.4	Turbulence . . . . .	11
3.4.1	Direct Numerical Simulation . . . . .	11
3.4.2	Turbulence models . . . . .	11
3.4.3	Model Coefficients . . . . .	14
3.5	Solving Methods . . . . .	15
3.5.1	Solving Code . . . . .	15
3.5.2	Differencing Schemes . . . . .	15
3.5.3	Solving Algorithm . . . . .	15
<b>4</b>	<b>Methods</b>	<b>16</b>
4.1	Case Study . . . . .	16
4.2	Image Based Meshing . . . . .	17

## CONTENTS

4.3	Initial Simulation . . . . .	19
4.4	Model Improvements . . . . .	19
4.5	Turbulence Effects . . . . .	21
4.6	Transient Effects . . . . .	22
4.6.1	Adjustable Timestep in pisoFoam . . . . .	23
4.7	Model Validation . . . . .	24
4.8	Model Convergence . . . . .	25
<b>5</b>	<b>Results</b>	<b>27</b>
5.1	Model Validation . . . . .	27
5.2	Porosity Calculations . . . . .	28
5.3	Visual Results . . . . .	29
5.4	Hydraulic Conductivity Calculation . . . . .	29
5.5	Computational Time . . . . .	33
<b>6</b>	<b>Conclusion</b>	<b>34</b>
<b>7</b>	<b>References</b>	<b>35</b>
<b>8</b>	<b>Appendix</b>	<b>37</b>
8.1	Appendix A: List of Figures . . . . .	37

## CHAPTER 1

# Introduction

## 1.1 Stormwater Management

It is becoming increasingly important to control what happens to stormwater rather than just directing it into the sewers along with the rest of the wastewater. This is due to legislation which is increasingly becoming more restrictive and putting a greater emphasis on sustainability.

In urban areas the water run off will contain large and small scale pollutants ranging from chemicals to particle matter, all of which must be filtered out. If this is done in the conventional manner it takes large amounts of energy which also puts unneeded pressure on sewerage plants. It can be done far more efficiently using many smaller scale processing plants which feed the water straight back into the water table. This also reduces the effect of putting large areas of tarmac on the surface preventing the water from entering the natural water system.

Due to these factors various legislation has come into effect in recent years or will be introduced soon, to this end more research is being done into the methods of filtering the water on site. In October 2000 the EU adopted the Water Framework Directive which requires surface water management across Europe to meet cleanliness criteria which have been specified. This was introduced into UK law in 2003 and has lead to the increase use of such systems to clean the water. These systems will become far more wide scale when the Sustainable Urban Drainage Systems legislation is introduced into UK in 2012, this legislation is designed to replicate natural water systems by using low cost solutions which have a low environmental impact.

## 1.2 Bioretention Systems

One of the types of methods of filtering the water at the point of collection is through the use of a Bioretention system. These are made up of various different grades of porous filter media to remove particulate matter and the use of natural processes such as the uptake of fluid into the root system of a tree to reduce the chemical elements.

### 1.2.1 *Hydro Filterra<sup>TM</sup>* System

An example of a Bioretention system in use is the *Hydro Filterra<sup>TM</sup>* which is produced by *Hydro International (UK)*. This is the system that will be analysed in this group project, an example of this system can be seen in figure 1.1.

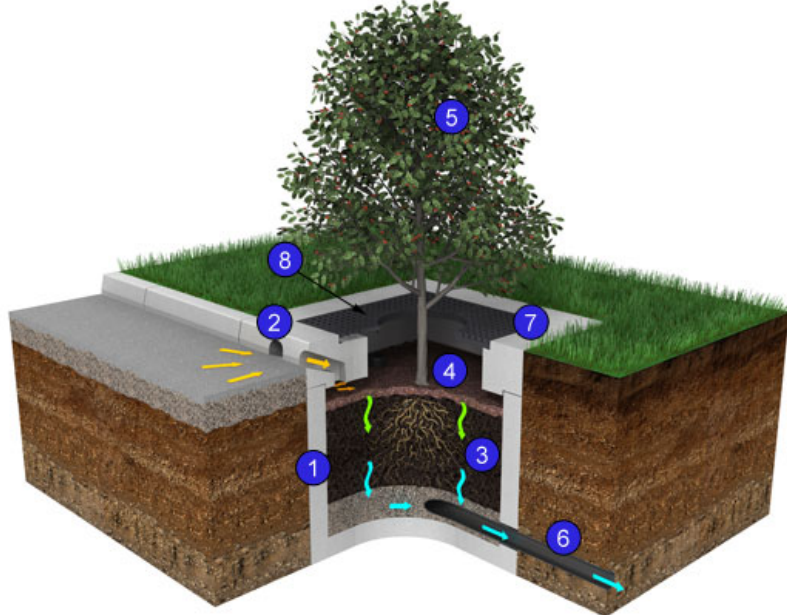


Figure 1.1: *Hydro Filterra<sup>TM</sup>* system[1]

The *Hydro Filterra<sup>TM</sup>* system has an advantage over other products due to using a specifically engineered filter media for the main filter section where the tree roots lie. Since the filter media is identical, each installation responds to rainfall in the same way. This filter material is between a mulch layer with energy dissipating stones at the top and a gravel layer at the bottom. Additionally, Due to each installation being identical maintenance is simplified due to there being common parts and design across all systems.

## 1.3 Water Flow Analysis

In order to gain more understanding of the filtration process and how it reacts to rainfall, it is necessary to investigate the hydrodynamic flow through the system.

The flow will be investigated both experimentally and by utilising computational models. The results from these two sections will then be used to determine flow parameters to enable any possible improvements to be made, this will enable improved filtration performance, greater water flow through the system, verification of the current design, optimisation of the casing structure and calibration of a large scale model containing the entire system.

### 1.3.1 Micro Scale Computational Analysis

In order to understand the properties of the porous media it is necessary to analyse them to determine their properties at a micro-level to enable analysis to be conducted on the full system at a macro-level.

This report investigates these properties at a micro-level by utilising modern techniques to create computational models of the flow through the system using pore geometries from real samples of the filter media.

This will be done by obtaining micro-CT scans of the filter media provided by *Hydro International (UK)* and taken from an active *Hydro Filterra™* site and using a technique called Image Based Meshing (IBM) to build a 3D model of the filter media. Then the Navier-Stokes equations will be solved for the flow around this model by using Computational Fluid Dynamics (CFD) which is an iterative solving technique.

In order to validate the results from the CFD, the results will be compared with experimental work done on a scaled version of the filter media which uses air rather than water to analyse the flow.

## 1.4 Project Aims & Deliverables

There are two sections within project aims & deliverables, firstly the group aims and deliverables for *Hydro International (UK)* for whom this project is conducted, as well as the individual aims & deliverables for this report.

### 1.4.1 Group Aims & Deliverables

The main aims & deliverables were identified through consultation with *Hydro International (UK)* and are outlined in the following list.

1. Develop current CFD approaches to characterise the filter media and verify these results experimentally
2. Develop a three dimensional model of the system; demonstrating interaction with the urban environment and outflow from the system including root effects
3. Analyse the current model in terms of the structural design of the casing
4. Consider how the system interacts with the hydrological cycle on a larger scale

### 1.4.2 Individual Aims & Deliverables

The initial aims & deliverables remained largely the same throughout the project due to its progression along with the initial project plan.

#### Aims

1. Create meshes for the media with the micro-CT data from the experimental team

## CHAPTER 1: INTRODUCTION

2. Analyse each sample using CFD to identify the flow parameters with the aim of incorporating turbulence models as required.
3. Compare CFD results with experimental data to determine model accuracy

### Deliverables

1. Deliver porosity to S. Pavey[2] and J. Please[3]
2. Deliver hydraulic conductivity to S. Winston-Gore[4]
3. Deliver a 3D model for Additive Layer Manufacturing (ALM) to J. Please[3]

The third aim & deliverable forms an extension to the project as it became apparent that this was a reliable method to validate the CFD model.

# CHAPTER 2

# Management

Since this was a group project there were two different areas of management; management of the group and personal management of the individual projects.

## 2.1 Individual Management

The Gantt chart in figure 2.2 was created at the beginning on the project, the project has successfully followed this throughout the year. Although, there were some significant changes due to other sections of the project progressing quicker than expected. Due to the first set of micro-CT scans being delivered significantly earlier than anticipated, instead of doing basic CFD on a packed bed produced using the computer aided design package *SolidWorks*, the project progressed directly onto image based meshing and running CFD on the models generated from the image based meshing.

The final outline of the project can be seen in the flow chart in figure 2.1. In the flow chart it can be seen how reliant this project was on the work from J. Please[3] which was all delivered ahead of time, it can also be seen that the results from this project were delivered into three other projects so it was important to ensure that the project kept to a schedule, although it is impossible to have an exact timetable with CFD due to the varying time it takes to run different simulations.

It was important to fully assess all health and safety risks involved with the project. While compared to projects involving laboratory work, sitting at a computer has few risks, there are still important factors to consider to ensure that long term health problems are not encountered due to extended periods of time sitting at a computer with bad posture and without taking breaks. To this end it was ensured that during any time period where computational work was completed regular breaks were taken and that at all times fully adjustable chairs were used so that the correct body posture could be maintained.

## 2.2 Group Management

To ensure the project remained on schedule weekly group meetings were held where detailed descriptions of the individual project progress was recalled so the group were aware of how each individual project was progressing. This also enabled the people that needed information from the other group members to have an idea of if their deliverable

## CHAPTER 2: MANAGEMENT

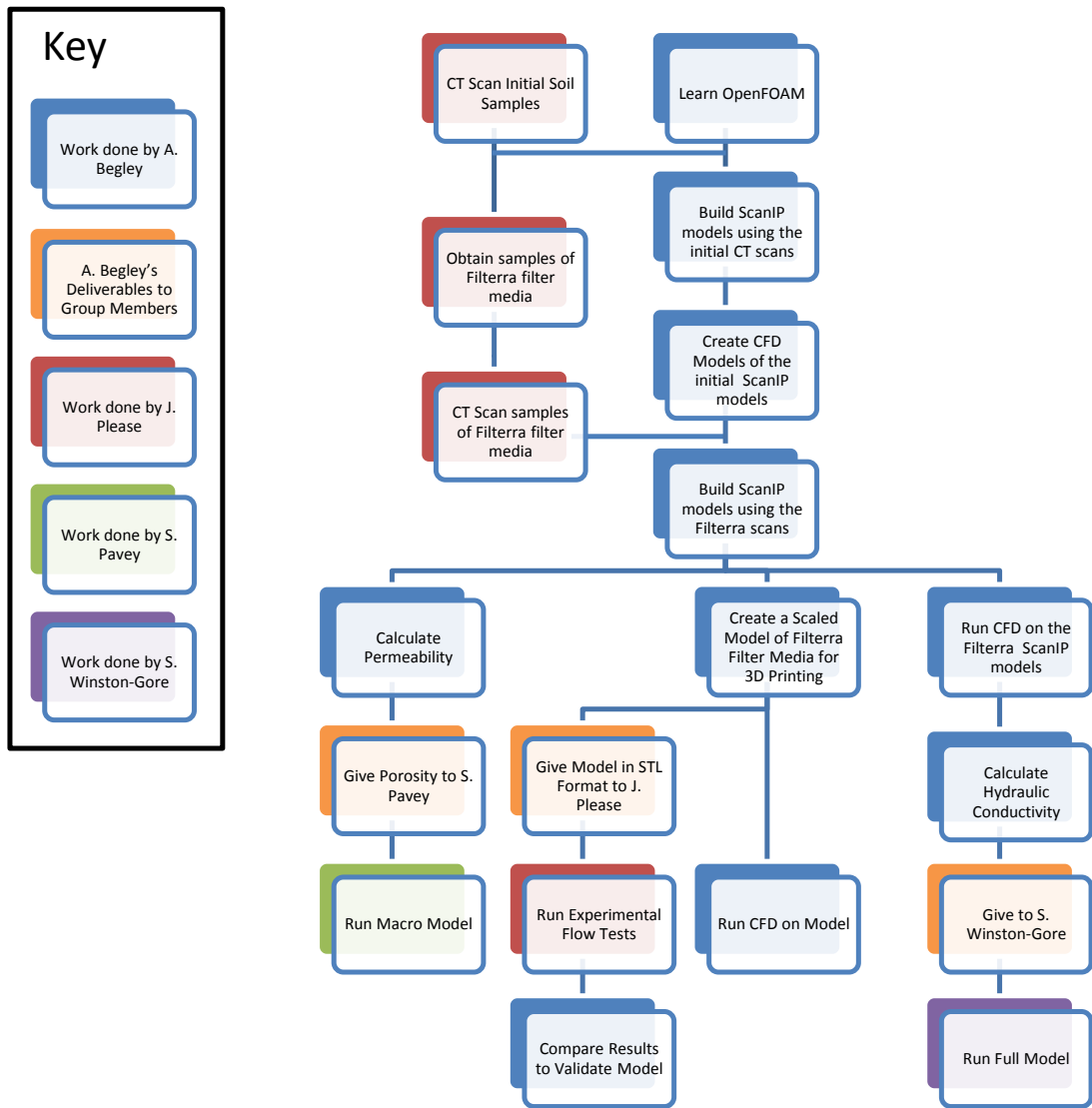


Figure 2.1: Flow chart of the project

was going to be late and if they needed it sooner than was expected.

As a group a few fixed positions were created such as treasurer and company liaisons officer but the weekly roles such as being secretary and chair rotated to balance the workload between the group.

This rotational group structure was recommended to us though it had some consequences as there was not one person managing the group who knew exactly how everyone was progressing compared to how much should have been done. This meant that there were periods where as a group productivity could have been higher.

A. Begley also set up a forum for the group so that minutes, files and results could be shared. Additionally, it was used to discuss any problems with the projects.

Because this project involved working on the intellectual property of *Hydro International (UK)* a formal agreement was necessary between *Hydro International (UK)* and the *University of Exeter* to ensure that none of the confidential data which was required for this project was used for other purposes.

## CHAPTER 2: MANAGEMENT

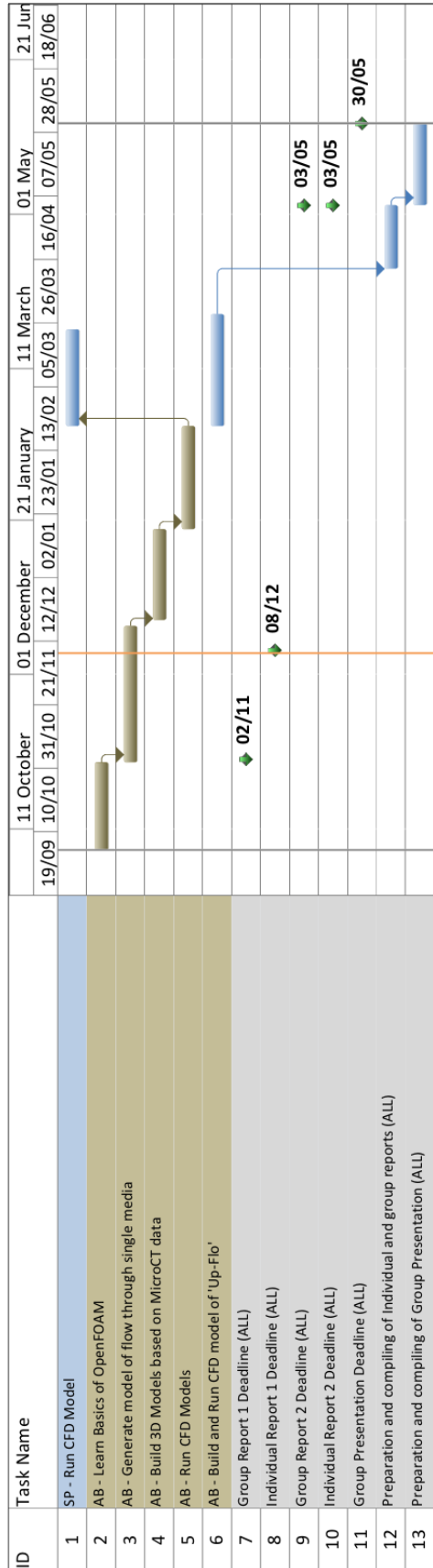


Figure 2.2: Gantt chart of the project

CHAPTER 3

## Review

The latest techniques used in this project such as IBM are constantly being used in new and innovative ways. Imaging techniques were used to create 3D models which accurately represented the pore geometries of filter media. These models were then solved for fluid flow using computational fluid dynamics, which had traditionally not been used on this scale. However there are many studies regarding packed beds and there are strong similarities between packed beds and soil/stone based filter media structures as can be seen in figure 3.1.

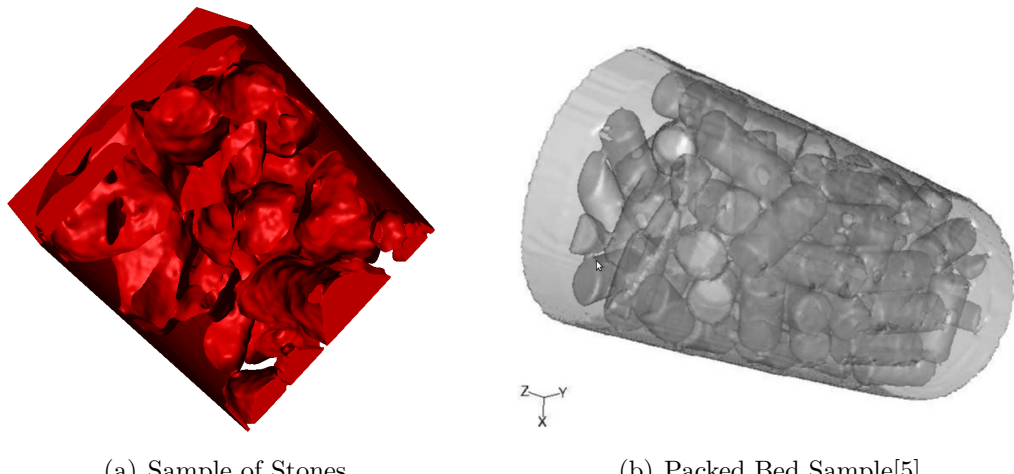


Figure 3.1: Similarity between a sample of stones and a packed bed

### 3.1 Packed Beds

While analysing fluid flow it is normally important to calculate the Reynolds number so the flow can be characterised as laminar, turbulent or in a transitional region in between. In this case the Reynolds number could be calculated using the particulate Reynolds number [5], which is defined in equation 3.1 where  $Re_{dp}$  is the particulate Reynolds number,  $\rho$  is the density,  $\mu$  is the dynamic viscosity,  $v$  is the superficial flow velocity which is the velocity that the fluid would flow at if the porous zone was not

present and  $d_p$  is the particle diameter.

$$Re_{dp} = \frac{\rho v d_p}{\mu} \quad (3.1)$$

When  $Re_{dp} < 10$  the fluid is in laminar flow, the fluid then enters the transitional region while  $10 < Re_{dp} > 300$  and the flow is turbulent when  $Re_{dp} > 300$  [6].

Since the equation 3.1 for particulate Reynolds number is based on equal sized spheres an equation had to be used to calculate the equivalent diameter of the particle if it were a sphere[7, 8], which can be seen in equation 3.2 where  $V_p$  is the volume of the particle and  $S_A$  is the surface area of the particle.

$$d_p = \frac{6V_p}{S_A} \quad (3.2)$$

Another method for calculating  $d_p$  uses an experimental technique as seen in the work by J. Please[3]. This technique involved obtaining an average particle diameter by sieve testing to determine how many particles are present at each diameter and taking a weighted average so assuming  $d_p = d_{50}$  where  $d_{50}$  is the median particle size diameter. However there were limitations with this approach, as the result will be skewed by including all the smaller particles which are not accounted for in the process of scanning and meshing the filter media sample.

Hydraulic conductivity and permeability can be calculated by using Darcy's law[9, 10] if the particulate Reynolds number is between 1 and 10[11]. Darcy's Law can be seen below in equation 3.3.

$$Q = K \frac{A(h_1 - h_2)}{L} \quad (3.3)$$

Hydraulic conductivity and permeability are related and it is possible to prove that they are proportional using Darcy's Law which results in equation 3.4[12] where  $K$  is hydraulic conductivity,  $\kappa$  is permeability and  $\gamma$  is the specific weight of the fluid.

$$K = \kappa \frac{\gamma}{\mu} \quad (3.4)$$

Equation 3.3 can be changed to use a pressure drop rather than a change in hydraulic head and superficial flow velocity rather than the flow rate by using the equations  $p = \rho gh$  and  $Q = vA$ . This results in the equation 3.5 where  $L$  is the specimen length in the direction of the flow.

$$\begin{aligned} K &= \frac{Q}{A} \times \frac{L}{h_1 - h_2} \\ &= v \times \frac{L}{\left( \frac{P_1}{\gamma} - \frac{P_2}{\gamma} \right)} \\ &= v \frac{L\gamma}{\Delta P} \end{aligned} \quad (3.5)$$

## 3.2 Image Based Meshing

In computational engineering it is a challenge to create an accurate 3D model especially for internal structures such as arteries or the internal pore geometry in packed beds

as such features are not externally visible and are very complex. Small changes to the model can have a large influence on the results of the computational analysis. This problem can be solved by using a method of imaging the subject such as micro-CT or MRI scanning, importing this data into a computer meshing package and using it to build a model. An example of how this can be used to model complex structures such as bones can be seen below in figure 3.2.

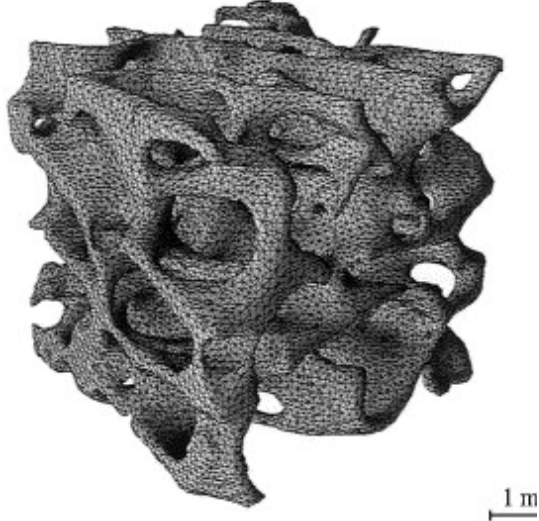


Figure 3.2: Finite element (FE) model of the femoral head specimen[13]

One approach to IBM involves taking a 3D model which has been built from imagery and then meshing the model which is usually an STL file by using another program such as snappyHexMesh which comes with *OpenFOAM*. This however usually only works on fairly simple geometry and is not a viable option for the complex geometries in packed beds.

Another approach is to combine these steps and make the 3D model and mesh the geometry at the same time. The method is utilised by the software *ScanIP* produced by *Simpleware*. The process of using *ScanIP* involved selecting which parts of the three 2D planes are required in the model by using various techniques, such as selecting regions based on their greyscale values or deselecting any regions which are not connected to the main flow. These are a mixture of semi-automatic and manual processes, this process of selecting the data required creates masks of the model. Once the masks are complete, the 3D model is then constructed and meshed simultaneously. This process creates meshes for various different CFD programs including *Fluent* and *OpenFOAM*. This process can mesh far more complicated geometry than using an external meshing program. *ScanIP* was first developed for FE analysis of bones for stress analysis[14] but as the process for creating a FE mesh is very similar to creating a CFD mesh the program could be easily adapted to add functionality for CFD software.

Using IBM with data from a micro-CT scan at the scale required for this project is a very innovative process which has previously had limited applications. This is due to lack of computing power previously available and the large amounts of RAM needed to created the meshes.

### 3.3 Computational Fluid Dynamics

Computational fluid dynamics is the process of solving of fluid flow problems using computers and it involves solving forms of the Navier-Stokes equations in one, two or three dimensions. In this case three dimensional flow is considered. Examples of available CFD codes include the commercial code *Fluent* or the open source code *OpenFOAM* which will be used for this project.

If the Reynolds number of the fluid flow is low enough to enable the fluid flow to be laminar then the laminar Navier-Stokes equations can be solved, these can be seen in equations 3.6 & 3.7.

$$\nabla \cdot \underline{u} = 0 \quad (3.6)$$

$$\frac{\partial \underline{u}}{\partial t} + \nabla \cdot \underline{u} \underline{u} = -\frac{1}{\rho} \nabla p + \nu \nabla^2 \underline{u} \quad (3.7)$$

### 3.4 Turbulence

The flow through the filter media could be turbulent under certain flow conditions and choosing how to model this is important as the effect of turbulence on the flow could be significant. Turbulence encompasses all quasi-random motions on all scales which obey the Navier-Stokes Equations. Although, fully solving the Navier-Stokes equations is not normally a viable option due to the available computer power so there are many methods of solving for turbulence.

#### 3.4.1 Direct Numerical Simulation

The only way of calculating the effects of turbulence without having to use numerical models is called Direct Numerical Simulation (DNS).

To solve a problem using DNS, the mesh has to be fine enough to fully resolve every turbulent eddy created and have a time step small enough to model the transient effects due to all the eddies. These small scales that must be fully modelled are known as the Kolmogorov micro-scales.

It is impractical to solve anything but basic models at low Reynolds numbers using DNS due to the high computational costs involved, as the number of calculations involved varies with  $Re^{9/4}$ . Due to this turbulence models have to be used which make some numerical assumptions.

#### 3.4.2 Turbulence models

In order to model turbulent flow the Navier-Stokes equations are altered by time or Reynolds averaging, this creates the Reynolds Averages Navier-Stokes (RANS) equations which can be seen in equations 3.8 & 3.9.

$$\nabla \cdot \bar{\underline{u}} = 0 \quad (3.8)$$

$$\frac{\partial \underline{u}}{\partial t} + \nabla \cdot \bar{\underline{u}} \bar{\underline{u}} + \nabla \cdot \underline{\underline{R}} = -\frac{1}{\rho} \nabla p + \nu \nabla^2 \bar{\underline{u}} \quad (3.9)$$

In equations 3.8 & 3.9 an additional term  $\underline{\underline{R}}$  is added which is Reynolds Stress, this is the effect due to turbulence on the mean flow, while the bar represents where a term has been averaged to become a Reynolds-averaged flow variable.

There are various methods of solving for  $\underline{\underline{R}}$  though the most common approaches are based on the Boussinesq eddy viscosity, which means that  $\underline{\underline{R}}$  can be modelled as shown in equation 3.10 where  $\nu_t$  is the turbulent viscosity.

$$\underline{\underline{R}} = \nu_t \nabla^2 \bar{u} - 2/3 k I \quad (3.10)$$

The turbulent viscosity is then modelled using two variables, either  $k$  &  $\epsilon$  for the kEpsilon model or  $k$  &  $\omega$  for the kOmega model. A large amount of the information in this section comes from the CFD Online Wiki[15].

This report investigated the three most common turbulence models, the  $k - \epsilon$ ,  $k - \omega$  and  $k - \omega SST$  model. These are all two equation models which includes two extra transport equations to represent the the turbulence of the flow.

### $k - \epsilon$ Model

The  $k - \epsilon$  model introduces two new variables where the first,  $k$ , is the turbulent kinetic energy and the second ,  $\epsilon$  is the turbulent dissipation which is the variable that determines the scale of the turbulence, while  $k$  determines the energy in the turbulence.

The  $k - \epsilon$  turbulence model has become a standard model due to it being an easier model to solve than the other standard models and has been used by Tierney *et al.*[16] & Gungal *et al.*[17]. It does have limitations as it is not as accurate near walls or for flows containing large adverse pressure gradients as other models, although it is accurate in free stream flows unlike other models.

The transport equations that are added for the  $k - \epsilon$  model can be seen in equations 3.11 & 3.12.

$$\frac{\partial}{\partial t} (\rho k) + \frac{\partial}{\partial x_i} (\rho k u_i) = \frac{\partial}{\partial x_j} \left[ \left( \mu + \frac{\mu_t}{\sigma_k} \right) \frac{\partial k}{\partial x_j} \right] + P_k + P_b - \rho \epsilon - Y_M + S_k \quad (3.11)$$

$$\frac{\partial}{\partial t} (\rho \epsilon) + \frac{\partial}{\partial x_i} (\rho \epsilon u_i) = \frac{\partial}{\partial x_j} \left[ \left( \mu + \frac{\mu_t}{\sigma_\epsilon} \right) \frac{\partial \epsilon}{\partial x_j} \right] + C_{1\epsilon} \frac{\epsilon}{k} (P_k + C_{3\epsilon} P_b) - C_{2\epsilon} \rho \frac{\epsilon^2}{k} + S_\epsilon \quad (3.12)$$

Where the standard model constants are;  $C_{1\epsilon} = 1.44$ ,  $C_{2\epsilon} = 1.92$ ,  $C_\mu = 0.09$ ,  $\sigma_k = 1.0$  and  $\sigma_\epsilon = 1.3$ .

The solutions to the equations 3.11 & 3.12 are then used to calculate the turbulent viscosity using the equation 3.13 which can then be input into equation 3.10 to solve R, for the RANS equations 3.8 & 3.9.

$$\mu_T = \rho C_\mu \frac{k^2}{\epsilon} \quad (3.13)$$

### $k - \omega$ Model

The  $k - \omega$  model again adds two variables,  $k$  and *omega* to the RANS equations. The term  $k$  is the turbulent kinetic energy as with the  $k - \epsilon$  model and the second is the

energy dissipation,  $\omega$ , which determines the scale of the turbulence. The first variable again determines the energy in the turbulence, this model has been used by Baker and Tabor[18] & Jan and Tobis[19].

The  $k - \omega$  model performs better than the  $k - \epsilon$  model near walls but is less accurate in free stream flows. Due to this the  $k - \omega$  model is not appropriate for external flow problems, though is suitable for internal flow problems such as through porous media.

The transport equations that are added for the  $k - \omega$  model can be seen in equations 3.14 & 3.15.

$$\frac{\partial k}{\partial t} + U_j \frac{\partial k}{\partial x_j} = \tau_{ij} \frac{\partial U_i}{\partial x_j} - \beta^* k \omega + \frac{\partial}{\partial x_j} \left[ (\nu + \sigma^* \nu_T) \frac{\partial k}{\partial x_j} \right] \quad (3.14)$$

$$\frac{\partial \omega}{\partial t} + U_j \frac{\partial \omega}{\partial x_j} = \alpha \frac{\omega}{k} \tau_{ij} \frac{\partial U_i}{\partial x_j} - \beta \omega^2 + \frac{\partial}{\partial x_j} \left[ (\nu + \sigma \nu_T) \frac{\partial \omega}{\partial x_j} \right] \quad (3.15)$$

Where these standard coefficients apply;  $\alpha = 5/9$ ,  $\beta = 0.075$ ,  $\beta^* = 0.09$ ,  $\sigma = 0.5$ ,  $\sigma^* = 0.5$  and  $\epsilon = \beta^* \omega k$ .

As with the  $k - \epsilon$  model the solutions to equations 3.14 & 3.15 are then used to calculate the turbulent viscosity, although in this case the equation 3.16 is used. As with the  $k - \omega$  model the turbulent viscosity is then used to calculate  $\underline{R}$ , which is then used to solve the RANS equations.

$$\nu_T = \frac{k}{\omega} \quad (3.16)$$

### $k - \omega SST$ Model

The  $k - \omega SST$  model is a blend of both models described above, where the best characteristics of each model are taken[20, 5] and the model is often given merit for its good behaviour in adverse pressure gradients and separating flows. However the  $k - \omega SST$  model produces larger turbulence levels in regions with large normal strain such as areas of large acceleration, though this effect is much less pronounced than with the standard  $k - \epsilon$  model.

The transport equations that are added for the  $k - \omega SST$  model can be seen in equations 3.17 & 3.18.

$$\frac{\partial k}{\partial t} + U_j \frac{\partial k}{\partial x_j} = P_k - \beta^* k \omega + \frac{\partial}{\partial x_j} \left[ (\nu + \sigma_k \nu_T) \frac{\partial k}{\partial x_j} \right] \quad (3.17)$$

$$\frac{\partial \omega}{\partial t} + U_j \frac{\partial \omega}{\partial x_j} = \alpha S^2 - \beta \omega^2 + \frac{\partial}{\partial x_j} \left[ (\nu + \sigma_\omega \nu_T) \frac{\partial \omega}{\partial x_j} \right] + 2(1 - F_1) \sigma_{\omega 2} \frac{1}{\omega} \frac{\partial k}{\partial x_i} \frac{\partial \omega}{\partial x_i} \quad (3.18)$$

These equations are solved using the following relationships and coefficients.

$$\begin{aligned}
 F_1 &= \tanh \left\{ \left\{ \min \left[ \max \left( \frac{\sqrt{k}}{\beta^* \omega y}, \frac{500\nu}{y^2 \omega} \right), \frac{4\sigma_{\omega 2} k}{CD_{k\omega} y^2} \right] \right\}^4 \right\} \\
 F_2 &= \tanh \left[ \left[ \max \left( \frac{2\sqrt{k}}{\beta^* \omega y}, \frac{500\nu}{y^2 \omega} \right) \right]^2 \right] \\
 P_k &= \min \left( \tau_{ij} \frac{\partial U_i}{\partial x_j}, 10\beta^* k \omega \right) \\
 CD_{k\omega} &= \max \left( 2\rho\sigma_{\omega 2} \frac{1}{\omega} \frac{\partial k}{\partial x_i} \frac{\partial w}{\partial x_i}, 10^{-10} \right) \\
 \phi &= \phi_1 F_1 + \phi_2 (1 - F_1) \\
 \alpha_1 &= \frac{5}{9}, \alpha_2 = 0.44, \beta_1 = \frac{3}{40}, \beta_2 = 0.0828, B^* = \frac{9}{100} \\
 \sigma_{k1} &= 0.85, \sigma_{k2} = 1, \sigma_{\omega 1} = 0.5, \sigma_{\omega 2} = 0.856
 \end{aligned}$$

As with the previous models the equations 3.17 & 3.18 are used to calculate the turbulent viscosity which can be seen for this model in equation 3.19. Again this is then used to solve for R which is then used to solve the RANS equations.

$$\nu_T = \frac{\alpha_1 k}{\max(\alpha_1 \omega, SF_2)} \quad (3.19)$$

### 3.4.3 Model Coefficients

All the turbulence models have coefficients which must be calculated for the boundary conditions. Determining the actual values is not possible, but there are reasonable approximations which are used. These values are used as exact values at the inlet, while along the walls a function uses them as an initial value to calculate how they vary. These initial values are calculated using equations 3.20, 3.21 and 3.22.

$$k = \frac{3}{2} (UI)^2 \quad (3.20)$$

$$\epsilon = C_\mu^{3/4} \frac{k^{3/2}}{l} \quad (3.21)$$

$$\omega = C_\mu^{-1/4} \frac{\sqrt{k}}{l} \quad (3.22)$$

Where  $U$  is the velocity at the inlet,  $I$  is the turbulence intensity,  $C_\mu=0.09$  & is a coefficient of the models and  $l$  is the turbulent length scale.

The turbulence intensity needs to be estimated and based on the information on CFD Online[15] a value of 2% was chosen as this is a case with a low-medium level of turbulence as this is a low speed flow with a low Reynolds number.

The turbulent length scale can be estimated based on the size of the system. It is not usually larger than the problem since eddies are usually of a smaller scale than the bounding domain.

## 3.5 Solving Methods

Methods for solving partial differential equations are an important consideration for producing reliable results in a CFD model, however it is often not possible to use the schemes that produce the most reliable results due to computing limitations or being extra sensitivity to numerical instabilities caused model limitations such as poor mesh quality and it is often the case that the methods are chosen because they are the only approach which solves the model.

### 3.5.1 Solving Code

There are many sets of code contained within *OpenFOAM* to solve different CFD cases and even some solutions for other types of problems which do not involve fluid flow but involve solving partial differential equations.

It was decided that for the steady-state solutions, a code called *simpleFoam* would be used as this uses the SIMPLE algorithm for RANS based flows.

For transient simulations a code called *pisoFoam* was used which utilises the PISO algorithm which is widely used for transient flows which is also a RANS based code.

As these are both RANS based codes it meant the same solver could be used under both laminar and turbulent conditions by changing the information specified in the case files.

### 3.5.2 Differencing Schemes

Differencing schemes determine how the values for all the variables are calculated at the cell faces. These values are calculated for cell centres, so to calculate the values at the cell faces interpolation is necessary as defined by the differencing schemes.

The most common and stable differencing technique is upwind differencing, where the value at the cell face is taken to be the upwind cell centre value, or  $\phi_f = \phi_c$ . Since upwind differencing is first order, it may produce severe numerical diffusion and introduce excessive numerical viscosity.

The most preferable differencing scheme is central differencing, where the cell face value is taken to be half way between the cell centre value for adjacent cells, or  $\phi_f = 0.5(\phi_c + \phi_d)$ . As a second order scheme it is inherently less stable than upwind and will often induce oscillation into the solution and make it unsolvable.

Another scheme is linearUpwind which is a blend of upwind and central differencing though the accuracy of the solution is limited based on the lowest order scheme.

### 3.5.3 Solving Algorithm

*OpenFOAM* has three solving algorithms to solve the Navier-Stokes equations. It is usual to start with Algebraic MultiGrid (GAMG) for pressure and smoothSolver for the other variables due to these having the greatest chance to solve problem however they do add an inherent inaccuracy. If possible it is best to progress to using a preconditioned (bi-)conjugate gradient technique, PCG/DIC for pressure and PBiCG/DILU for everything else.

## CHAPTER 4

# Methods

There are four main methods used in this project: Using image based meshing to create the models for CFD in *ScanIP*; setting up the model to run in *OpenFOAM*; improving both the model from *ScanIP* and the settings for *OpenFOAM* and finally, validating the model. Models were run on filter media which was obtained from the case study and also on the sample that was supplied by *Hydro International (UK)*.

## 4.1 Case Study

A large part of this project was based on a case study of an active *Hydro Filterra<sup>TM</sup>* site which was installed on an industrial site in Barry, South Wales.

The *Hydro Filterra<sup>TM</sup>* unit at this location had been installed for over a year at the time of the site visit. The visit was undertaken to increase understanding of the situation where this type of unit is installed as well as enabling samples of the filter media to be taken, as shown in figure 4.1.



Figure 4.1: Sample of filter material taken from an active *Hydro Filterra<sup>TM</sup>* site

## 4.2 Image Based Meshing

Samples of filter media were collected and micro-CT scanned by J. Please[3] these samples were contained within 20mm test tubes. The first sample was taken from an active *Hydro Filterra™* site as shown in figure 4.1 and another that was provided by *Hydro International (UK)*. Both the models went through the same process to generate the final models though this section will focus on the sample that from the case study.

Scan data was exported in the form as DICOM images which can be directly imported into *ScanIP*. The original data from the scans had a voxel size of 0.022784mm which was far too detailed to create a model using the available 16GB of ram. Therefore the data was re-sampled down to a voxel size of 0.05mm.

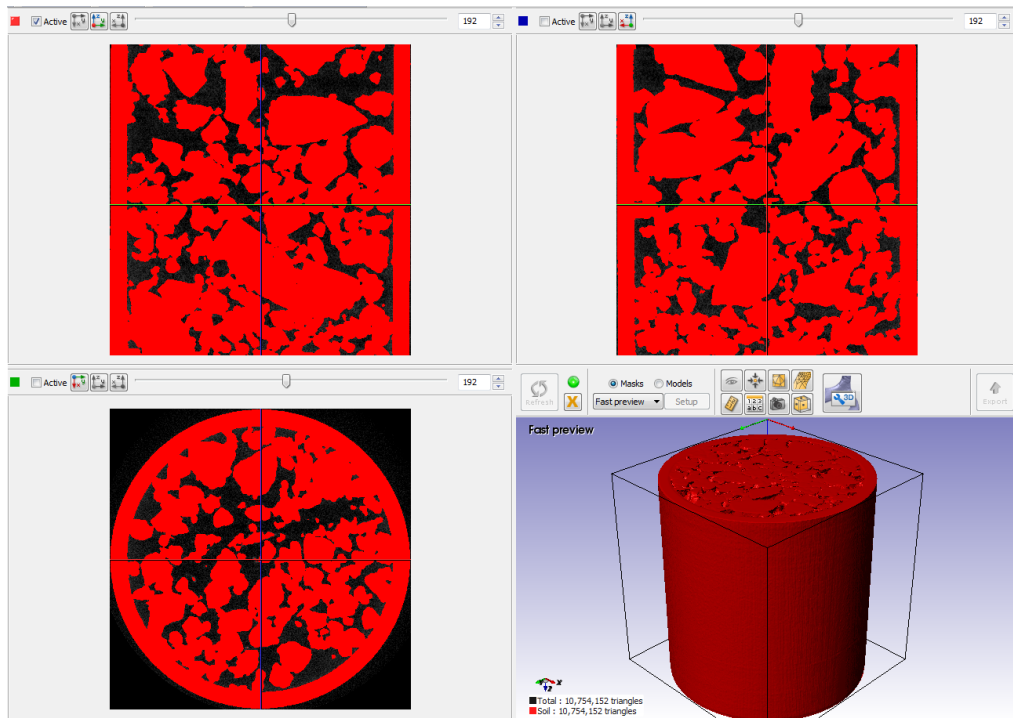


Figure 4.2: Selection of filter media in *ScanIP*

The images from the micro-CT scan are in a greyscale format where, depending on the density of the material the grey scale value changes. It is possible to select the particles of the filter material by specifying a grey scale range which includes every solid particle. This was achieved by selecting everything with a value between 82 and 255 where 255 is white and 0 is black. The result of this can be seen in figures 4.2 and 4.3.

Figure 4.2 shows the selection of the filter media in *ScanIP* cut along each axis and the full 3D model that this creates, which includes the test tube. Figure 4.3 shows the model from figure 4.2 cut in half to display the the filter media grains.

The volume of fluid is required for construction of a CFD model and care was taken to ensure that this was selected for the model. Therefore, the selected filter region was inverted. If the entire sample of filter media was used to construct the model, packing effects would be apparent around the edges of the sample due to the test tube. Therefore, a core sample of 255 pixels or 12.5mm in diameter was selected. This can be seen in figure 4.4

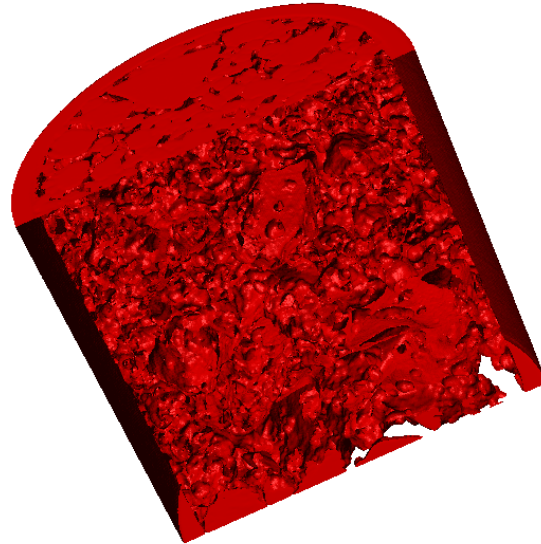


Figure 4.3: Selection of filter media in ScanIP in 3D

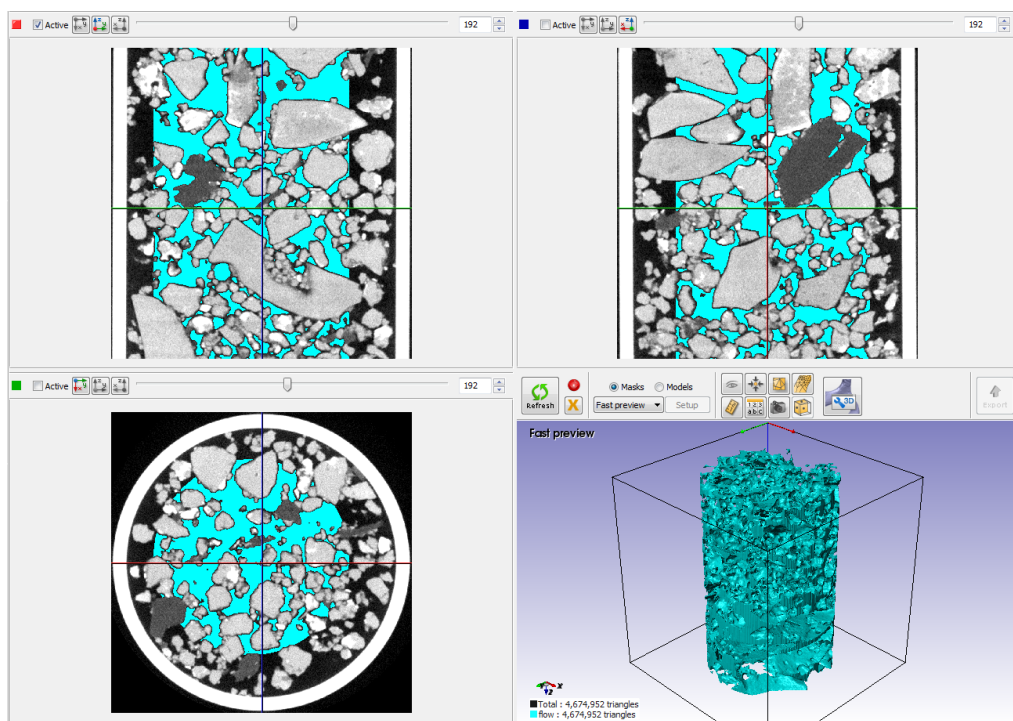


Figure 4.4: Selection of flow in *ScanIP*

This was then converted for a CFD analysis using *ScanIP*'s robust meshing algorithm called *+FE Grid* which is able to mesh geometries. However, due to the complex nature of this mesh some extra mesh quality improvement steps were needed to be enabled in the advanced options to reduce the number of skewed and non-orthogonal cells. This created a mesh with 22million cells.

## 4.3 Initial Simulation

The mesh from the previous section was imported into *OpenFOAM* where it was modelled with an inlet velocity and a calculated pressure at  $z_{\max}$ . At  $z_{\min}$  the outlet velocity was calculated and a pressure of zero was specified. This was so that the pressure drop across the model could be calculated. Both the outer edge of the mesh and internal filter material boundaries were treated as walls with zero velocity at the surface.

The velocity at the inlet was chosen to be  $3.5 \times 10^{-4}\text{m/s}$ . This was specified according to information obtained directly from *Hydro International (UK)* stating that on the unit which has a cross sectional area of  $1.2\text{m} \times 1.2\text{m}$  there is a maximum volumetric flow rate of  $1.83\text{m}^3/\text{h}$  which converts into the velocity specified above. The value of  $1.307 \times 10^{-6}\text{m}^2/\text{s}$  was chosen for kinematic viscosity due to the mean temperature at the location of the case study being  $10^\circ\text{C}$ [21].

The model was solved with a mixture of linearUpwind and central differencing which as discussed in section 3.5.2, is known to be the most reliable differencing scheme. The model was also successfully solved using the solving schemes PCG/DIC for pressure and PBiCG/DILU for the velocity which are known to be the most reliable solvers within *OpenFOAM*.

The model was run in parallel. In order to determine the optimum number of threads a small test was undertaken. This was necessary as modern computers have virtual cores enabled due to Hyper Threading as well as real cores. This was tested by running the motorBike tutorial, using a varying number of threads on a computer with an Intel Core i7 processor which has 4 cores and 8 threads. The results from this can be seen in table 4.1.

Table 4.1: Time taken to run the motorBike tutorial

Number of Threads	Time (s)
1	801
2	557
4	501
6	519

From the results in table 4.1 it can be seen that the time taken to mesh and run the model is optimum at 4 threads which is equal to the number of real cores in the processor. It was decided that the threads available from hyper threading would be ignored for running models.

This model was run on the computer with two six core Xenon processors with hyper threading so 12 cores were used for the simulation which ran for 300 iterations with an average time of 106 seconds per iteration. A view of the pressure and velocity profiles for this model can be seen in figure 4.5.

## 4.4 Model Improvements

After the initial model had been solved two main improvements were identified to make to the model to create an accurate representation of flow in the filter media and give

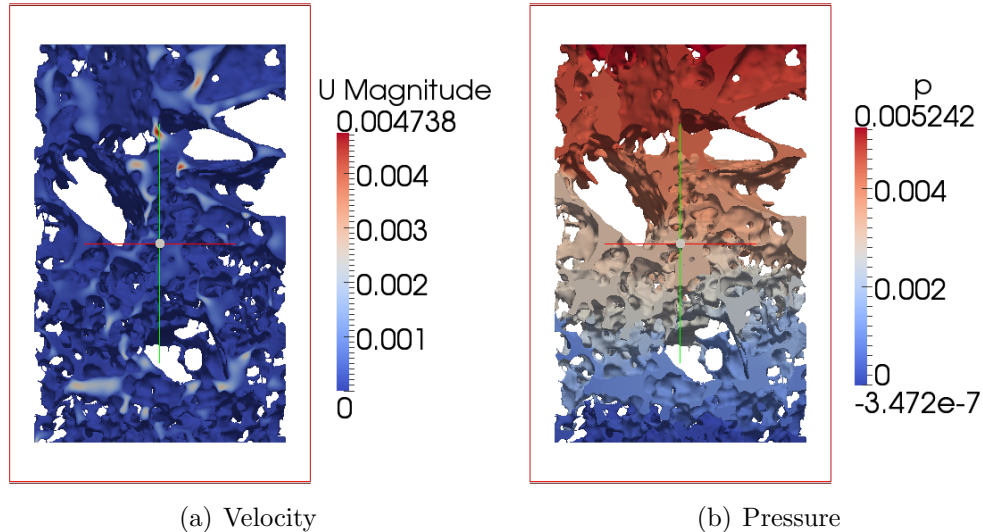


Figure 4.5: Results for the initial model

usable results for calculating hydraulic conductivity.

The first improvement was in the image based meshing process. In order to calculate hydraulic conductivity using equation 3.5 it is necessary to know the superficial flow velocity. This was not possible with the previous setup as it specifies that at the initial gaps in the porous media, the flow is the inlet velocity, rather than the flow over the entire cross sectional area of the model being this value. To solve this an inlet and outlet pipe was added onto either side of the model as can be seen in figure 4.6.

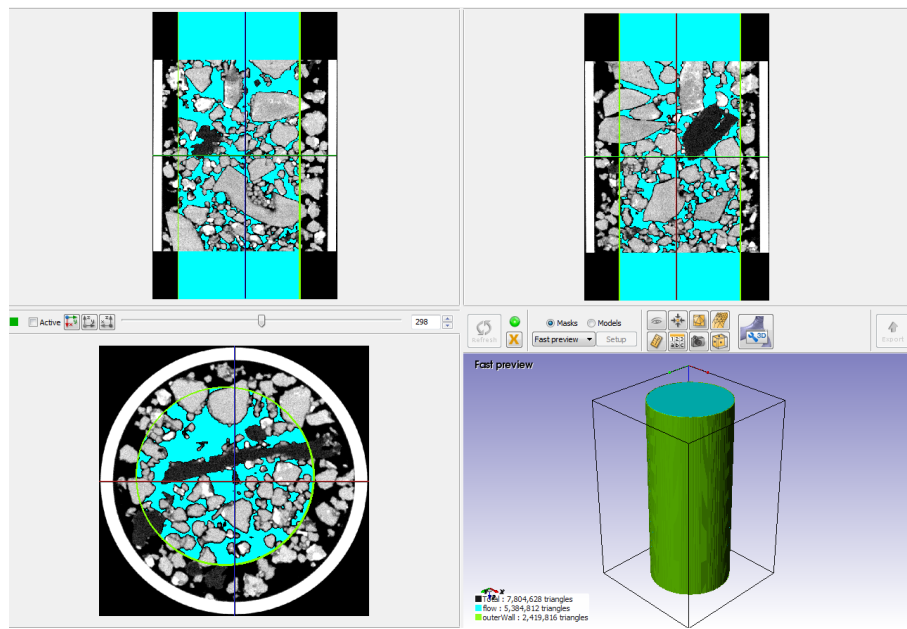


Figure 4.6: Selection of flow in *ScanIP*

This final model created a very dense mesh with a significantly larger volume than the initial mesh. This caused the total number of cells to increase to over 22 million. This made the choice of computer for this simulation an important consideration due to the

simulation requirements of around 18GB of ram for a successful solution. The initial model was solved on a 12 Xeon because it was faster than other available options due to the ability to split the model over 12 cores. This model had to be solved on that computer it being the only available machine with more than 16GB of ram.

The second improvement was to change the boundary condition for the flow around the edge of the model to a condition where the wall made no difference to the flow. In order to do this, the sample was encased in a tube in *ScanIP* as seen in figure 4.6 and then the boundary condition for where the flow meets this wall was set to slip. This condition specifies that if the flux is scalar then the boundary condition is set to zeroGradient while if the flux is a vector then normal components have a fixed value of zero and tangential components are set to zeroGradient. The results of these changes can be seen in figure 4.7.

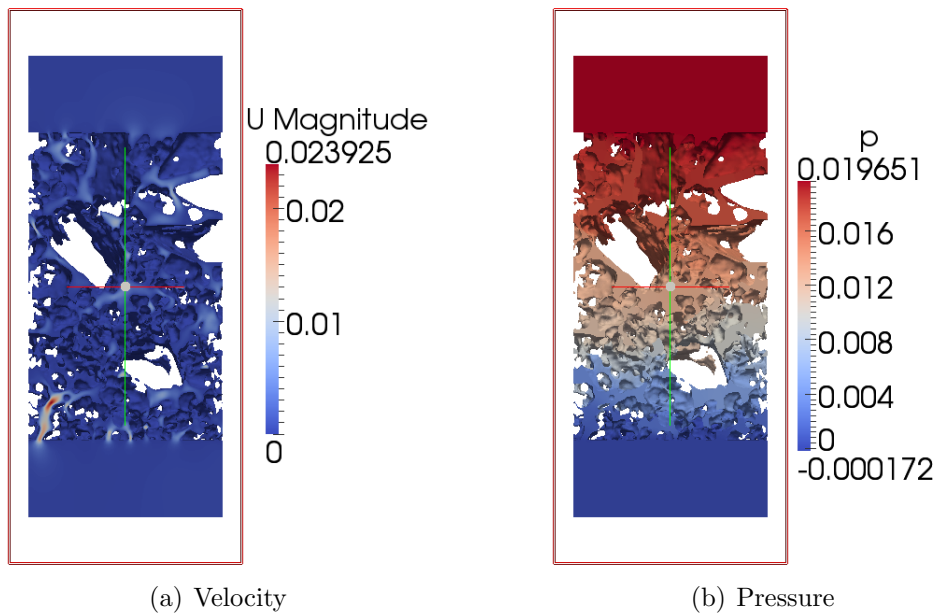


Figure 4.7: Results for the improved model

## 4.5 Turbulence Effects

As indicated in sections 3.1 and 3.4, modelling turbulence is highly important for flows with high Reynolds numbers. The model was being run for a very low Reynolds number as can be seen in equation 4.1 which is taken from equation 3.1

$$Re_{dp} = \frac{1000 \times 0.00035 \times 0.003682}{1.307 \times 10^{-3}} \\ Re_{dp} = 0.99 \quad (4.1)$$

As  $Re_{dp} < 10$  then turbulence is not be expected, although localised areas could have a higher Reynolds number due to the varying size of particles in this case. This is because it is not a uniform packed bed, and it is noted that a small increase in velocity would move the model into the transition period.

In order run the simulation with turbulence models values for the three co-efficients ( $k$ ,  $\epsilon$  &  $\omega$ ) had to be calculated using equations 3.20, 3.21 and 3.22 as can be seen below.

$$\begin{aligned} k &= \frac{3}{2} (0.00035 \times 0.02)^2 \\ k &= 7.35 \times 10^{-11} \\ \epsilon &= 0.09^{3/4} \frac{(7.35 \times 10^{-11})^{3/2}}{0.07 \times 12.5 \times 10^{-3}} \\ \epsilon &= 1.18 \times 10^{-13} \\ \omega &= 0.09^{-1/4} \frac{\sqrt{7.35 \times 10^{-11}}}{0.07 \times 12.5 \times 10^{-3}} \\ \omega &= 7.18 \times 10^{-4} \end{aligned}$$

Unfortunately while attempting to run this model with any of the turbulence models, the simulation crashed due to a numerical instability which caused a 'floating point exception'. This could be due to mesh errors as some of the cells were very skewed and non-orthogonal or it could be associated with the geometry being extremely complex, causing the interactions with the different flows to be too complicated for the model. This should however, not too much of a problem as the work by Baker *et al.* [5] showed that the turbulence model had little effect on the flow, even in the regions where the particulate Reynolds number approached 5000, thus reasonable conclusions can be made from laminar studies.

## 4.6 Transient Effects

When running the improved model from section 4.4, the residuals for the simulation decreased for the first 150 iterations as expected but then increased slightly and began to oscillate as can be seen in figure 4.8.

This is due to an instability which is possibly due to transient effects in the flow as it passes through the filter media despite the Reynolds number being significantly lower than what would be expected for turbulent flow. To determine how these transient behaviours effected the pressure drop it was necessary to run a simulation which was not steady-state. This was done using pisoFoam. It was discovered that unless the time-step for each iteration was tiny, then the Courant number would go too high and the simulation would crash.

The Courant-Friedrichs-Lowy condition is a condition for convergence while solving partial differential equations using finite differencing and is described by equation 4.2 where  $u$  is the velocity,  $\Delta t$  is the time-step,  $\Delta x$  is the length interval and  $C$  is a dimensionless constant which is dependant on the equation that is being solved.

$$\frac{u\Delta t}{\Delta x} \leq C \quad (4.2)$$

Where the dimensionless number,  $c$ , shown in equation 4.3 is the Courant number. For solving the Navier-Stokes equations the Courant number must remain below 1 and ideally should remain below 0.5 to enable the solution to converge.

$$c = \frac{u\Delta t}{\Delta x} \quad (4.3)$$

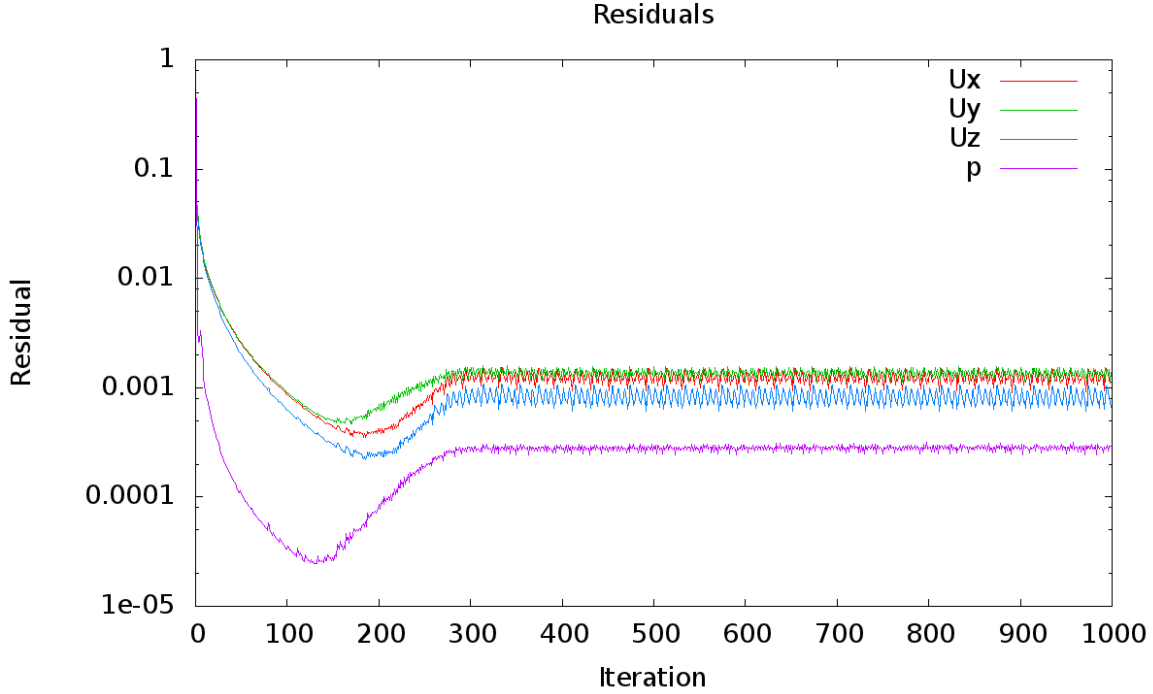


Figure 4.8: Graph of the residuals

#### 4.6.1 Adjustable Timestep in pisoFoam

It can be seen from equation 4.3 that to lower the Courant number the time-step needs to be reduced. This can either be done by guessing a small time-step which will often be too low causing unnecessary iterations, and will mean that if a numerical instability develops the Courant number could dramatically increase.

It is possible to overcome this problem in *OpenFOAM* as it has the ability to change the time step based on Courant number, however it is not included in pisoFoam by default so it was necessary to edit the code and recompile it.

The code that was added to pisoFoam.C can be seen below.

```
int main(int argc, char *argv[])
{
    #include "setRootCase.H"

    #include "createTime.H"
    #include "createMesh.H"
    #include "createFields.H"
    #include "initContinuityErrs.H"
    #include "readTimeControls.H" //Added

    // * * * * * * * * * * * * * * * * * * * * * * * * * * * * * * * * * * * //

    Info<< "\nStarting time loop\n" << endl;

    //while (runTime.loop()) //Removed
```

```

while (runTime.run()) //Added
{
    #include "readPISOControls.H" //Added
    #include "CourantNo.H" //Added
    #include "setDeltaT.H" //Added
    runTime++; //Added
    Info<< "Time = " << runTime.timeName() << nl << endl;

    //##include "readPISOControls.H" //Removed
    //##include "CourantNo.H" //Removed
}

```

Once this had been achieved the new pisoFoam could be run and by adding these lines to controlDict the time step would adjust to keep the Courant number below 0.5.

```

adjustTimeStep yes;
maxCo          0.5;
maxAlphaCo     0.5;
maxDeltaT      1;

```

Despite all this modification of source code, the system could not be solved. The constantly raising Courant number reduced the time-step to levels such as 1e-10 which meant that the simulation would never progress in a reasonable time-frame. This is likely due to problems with the mesh as discussed in section 4.5.

## 4.7 Model Validation

No computational method of analysis is completely reliable due to the uncertainty of the model, the user defined model inputs and numerical error. In this case there is also another layer of uncertainty due to the need to micro-CT scan the filter media and build up a model using IBM where it was necessary to choose which parts of the model were a solid particles and which were voids which lead to a loss of detail.

In order to validate the model, experimental work was completed similar to that completed by Baker *et al.*[5] and Narsilio *et al.*[9] where the model analysed using CFD was built using Additive Layer Manufacturing (ALM).

The experimental work completed by J. Please[3] required a model of the filter media within a skin. The 3D model to be printed was specified as 99mm in diameter including the skin and 100mm deep so a section had to be taken out of the scan data which was then scaled up by 7.7646 as can be seen in figure 4.9.

As the experimental work was conducted using air, CFD was also run on the new scaled up model with air at comparable velocities, so that a direct comparison between the CFD and experimental results could be made. Since the new CFD model contained a smaller volume of filter media, this model also contained less cells than the previous models. This enabled the model to be solved on other computers due to the lower RAM requirements as the number of cells decreased to 19million. Due to this factor and resource limitations on the 12 Xeon computer, these simulations were run on a 4 core Intel Core i7 running at 4.6Ghz with 16gb of ram.

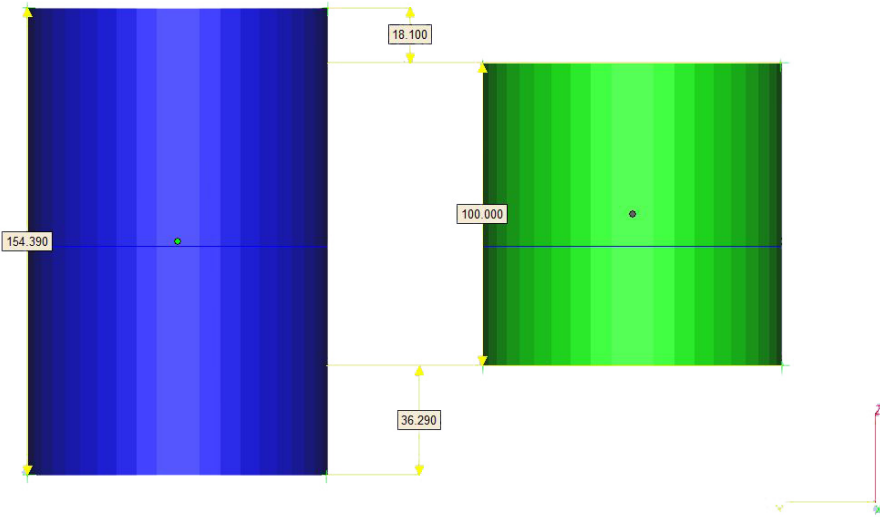


Figure 4.9: Showing the part of the model that was created using ALM

## 4.8 Model Convergence

It is important to insure that the CFD models run for enough iterations to allow the results to become converge on a solution.

To check for convergence it is necessary to chose a variable which the model outputs and record its value at every time step. This value should then be plotted against number of iterations and once the value stops changing as the iterations increase the solution has converged.

In this case the pressure drop across the model was chosen as the method for checking convergence, as this is the variable required for model validation as well as calculating hydraulic conductivity. Using *OpenFOAM* it is possible to have the solver output a value of pressure at a specific point in the model every iteration by using the code below in the controlDict file.

```

functions
{
    pressureDrop
    {
        type probes; // Type of functionObject
        // Where to load it from (if not already in solver)
        functionObjectLibs ("libsampling.so");
        probeLocations // runTime modifiable!
        (
            (0.045 0.045 0.19)
        );
        // Fields to be probed. runTime modifiable!
        fields
        (

```

```
    }  
};  
}
```

The point chosen to check for convergence was the pressure at the center of the inlet which is calculated based on a pressure of zero at the outlet, in the case of the code above it was for the case used in model validation.

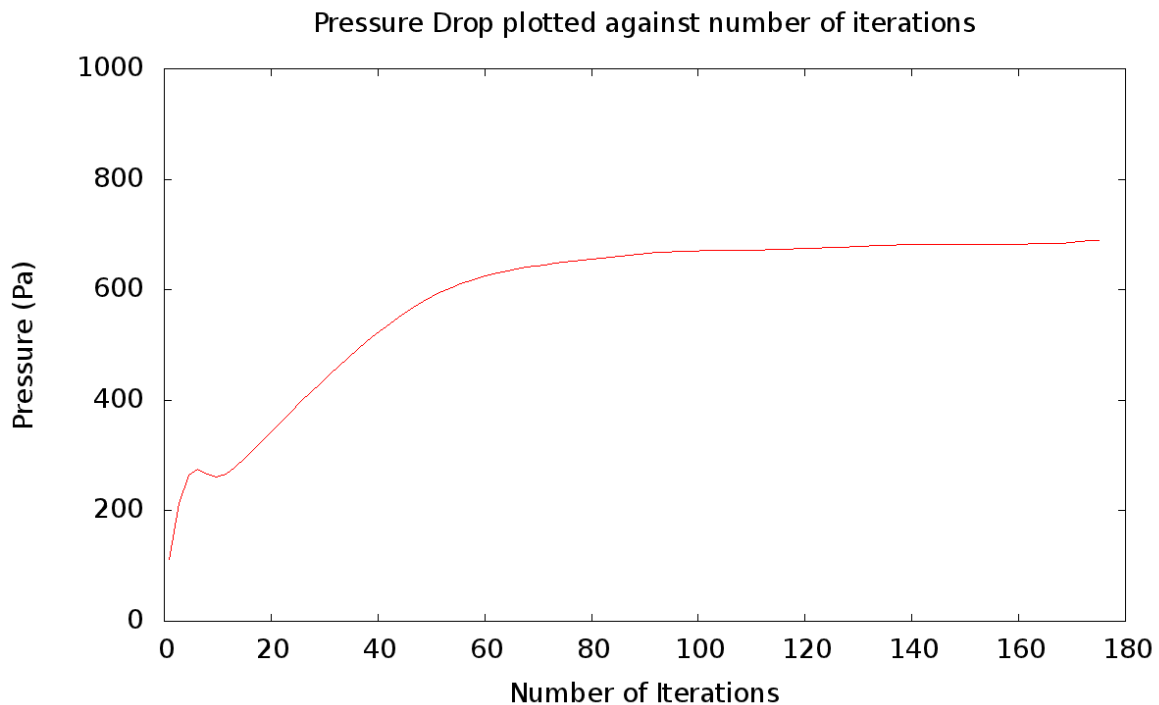


Figure 4.10: Pressure drop plotted against number of iterations to show convergence

From figure 4.10 it can be seen that the pressure drop over the filter media stops increasing after 100 iterations. So after 100 iterations the solution has converged. This meant that time could be saved while running the remaining simulations as they only needed to be run for 125 iterations.

## CHAPTER 5

# Results

Validation of the flow having been displayed is perhaps the most important section. This the model validation exercise is discussed first, with the results outlined later in chronological order.

## 5.1 Model Validation

CFD was conducted on the model with a particulate Reynolds numbers between 27 and 813. This range was chosen in order to achieve comparable data with the experimental work done by J. Please[3]. The lowest Reynolds number that the experimental work could test was around 400 due to limitations with the apparatus.

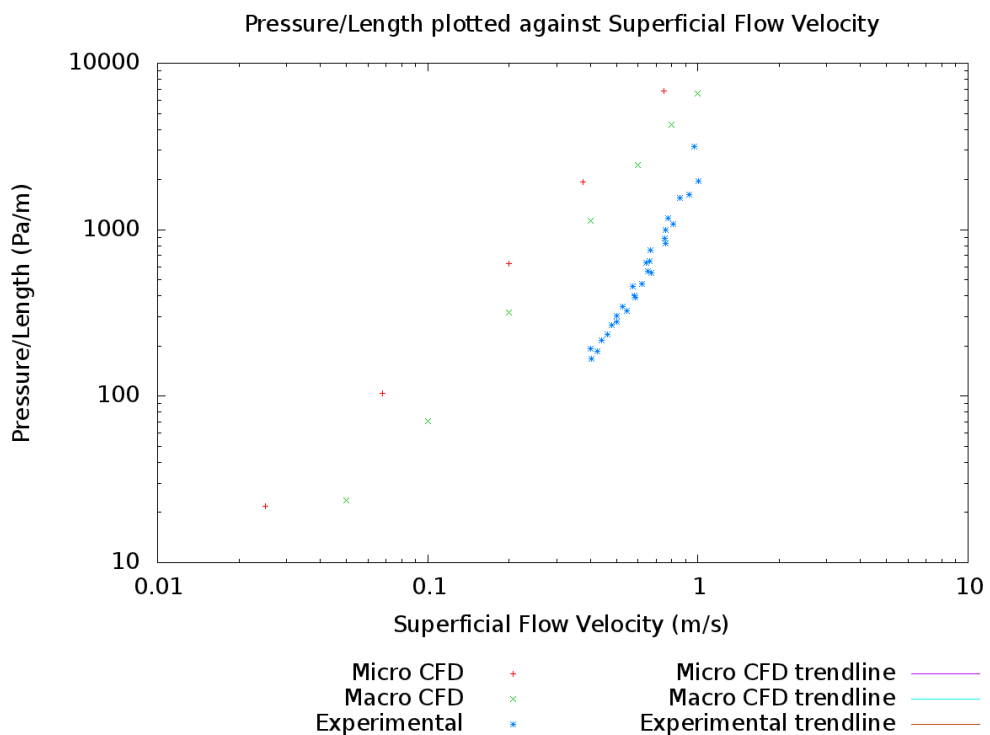


Figure 5.1: Comparison of P/l against Reynolds number for microCFD, macroCFD and experimental data

## CHAPTER 5: RESULTS

Results were achieved by J. Please[3] were plotted on a dimensionless graph alongside experimental flow testing of a packed bed proved that fluid flows through the filter media do not behave as a packed bed due to discrepancies between the trends. This conclusion also implies that the calculation that had been used for Reynolds number in equation 3.1 is invalid for flow through the filter media. This is due to the length scale used for this Reynolds number being for packed beds. However, it is noted that the calculation for hydraulic conductivity in equation 3.5 is still valid as this was based on Darcy's law which is determined experimentally for any porous media rather than packed beds.

The results from this CFD model, the macro CFD model and the experimental work can be seen in figure 5.1.

It can be seen from figure 5.1 that all three sets of results follow the same trend, though the values are significantly different. The macro CFD work by S. Pavey[2] has shown that a small change in particle diameter has a large effect on the results and that by changing the particle diameter by a believable amount the macro CFD results line up with the experimental results.

The CFD results from this project are however an order of magnitude too big but do follow the correct trend. Thus it is concluded that current models are not accurate for flow through the filter media. This could be due to the assumption that a turbulence model is not needed for CFD of flow through a packed bed from the work by Baker *et al.*[5]. As it has been proven, flow through the filter media does not act in the same way as flow through a packed bed. Thus a turbulence model may be required and the absence of such a model may be the cause of the inaccuracy of this model.

Another potential cause of error in the model is due to air being a compressible fluid, modelled here as an incompressible fluid. However this is highly unlikely to be the cause of the error as it is widely accepted that until the velocity of air reaches a Mach number of 0.3 it behaves as an incompressible fluid and the velocities that are found in this model are significantly below this velocity.

## 5.2 Porosity Calculations

The work done by S. Pavey[2] required the porosity to be calculated from the model generated by IBM, porosity is calculated by using equation 5.1 where  $\phi$  is the porosity,  $V_V$  is the volume of void space,  $V_S$  is the volume of solid matter and  $V_T$  is the total volume of the material.

$$\phi = \frac{V_V}{V_T} = 1 - \frac{V_S}{V_T} \quad (5.1)$$

Using *ScanIP*, it was possible to output the volume where the fluid would flow, though this included the inlet and outlet areas of the model. From this information it was possible to calculate  $V_S$  by subtracting the total fluid volume from the total volume of the model. This was required for both the experimental model and the model containing all the scan data due to the anisotropy of the filter media.

This lead to porosity values of 0.2284 for the model containing the full set of data from the micro-CT scan of the filter media from the case study and 0.2497 for the experimental model.

Using the IBM methods included the tool called 'FloodFill' the fluid domain was built only with the fluid paths through the filter media and no isolated void spaces. Due

to this, the porosity calculated by this method is the effective porosity rather than the total porosity which was calculated by J. Please[3] to be 0.3155.

### 5.3 Visual Results

A pictorial representation of the pressure drop and velocity profiles can be seen for the sample of filter media taken from the case study in figure 5.2. In this case the inlet velocity was  $3.5 \times 10^{-4}$ m/s. By inspection, it can be seen how complicated the flow paths are due to the small geometry within the filter media.

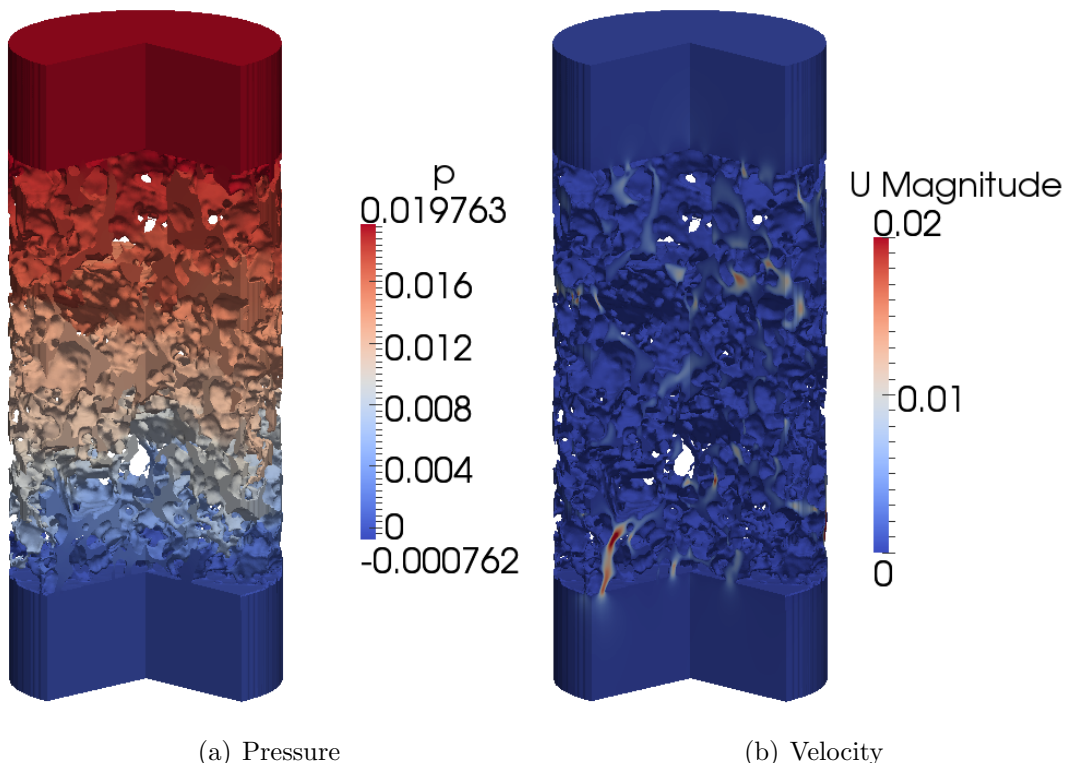


Figure 5.2: CFD Results from the filter media taken from the case study

The results from the sample of filter media obtained from *Hydro International (UK)* can be seen in figure 5.3, the inlet velocity in this case was 0.0213m/s which causes the larger pressure drop. By comparing figures 5.2 and 5.3 it can be seen that the grain size of the filter media supplied by *Hydro International (UK)* is of a significantly greater size than the filter media that was taken from the case study. This was explained through correspondence with *Hydro International (UK)*, who supplied the filter media, who informed the group that this batch was lacking in organic content which would cause this increase in average grain size.

### 5.4 Hydraulic Conductivity Calculation

Hydraulic conductivity as calculated using the equation 3.5 is based on Darcey's Law. Darcey's law is only valid for ranges of Reynolds numbers between 1 and 10 as stated in

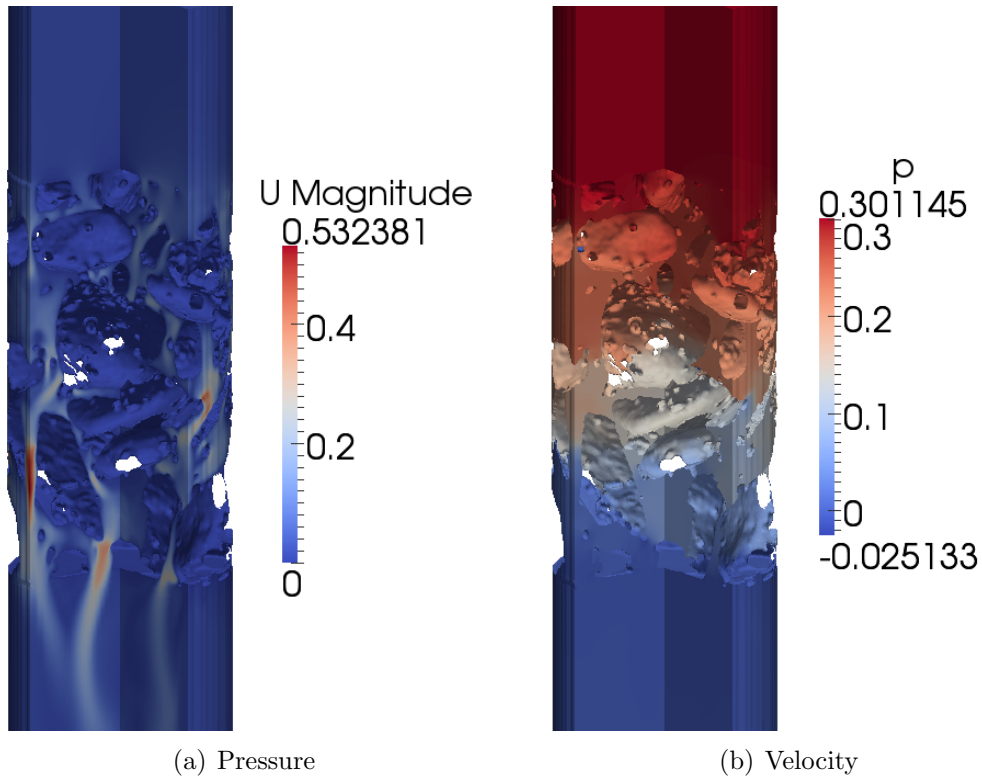


Figure 5.3: CFD Results from the filter media supplied by Hydro

section 3.1. Due to the filter material not acting as a packed bed, it is unknown what length scale to use so a Reynolds number could not be calculated.

To solve this problem the simulation was run multiple times on the filter media taken from the case study. Once on the full geometry from the micro-CT scan and twice on the section used for the experimental work at various superficial flow velocities. It was expected that there would be a range where changing the superficial flow velocity had no effect on the hydraulic conductivity due to both velocities being in the range that Darcey's law is valid.

The change in pressure over the length of the model can be seen in figure 5.4 where the inlet and outlet sections display a constant pressure and as the flow passes down through the model the pressure decreases. The gaps in the graph occur wherever the data line passes through filter media rather than the fluid domain, in these locations there is no pressure value in the model.

The initial model was run with a superficial flow velocity of  $3.5 \times 10^{-4}$  over a length of 0.0198836m which gave results as can be seen in equation 5.2.

$$K = \frac{0.00035 \times 0.0198836 \times 1000 \times 9.8}{0.0196}$$

A scaled down version of the experimental model was then run at velocities of  $2.13 \times 10^{-2}$ m/s and  $2.84 \times 10^{-3}$ m/s which acted over a length of  $0.1 \times \frac{12.75}{99}$  giving the results in equations 5.3 & 5.4.

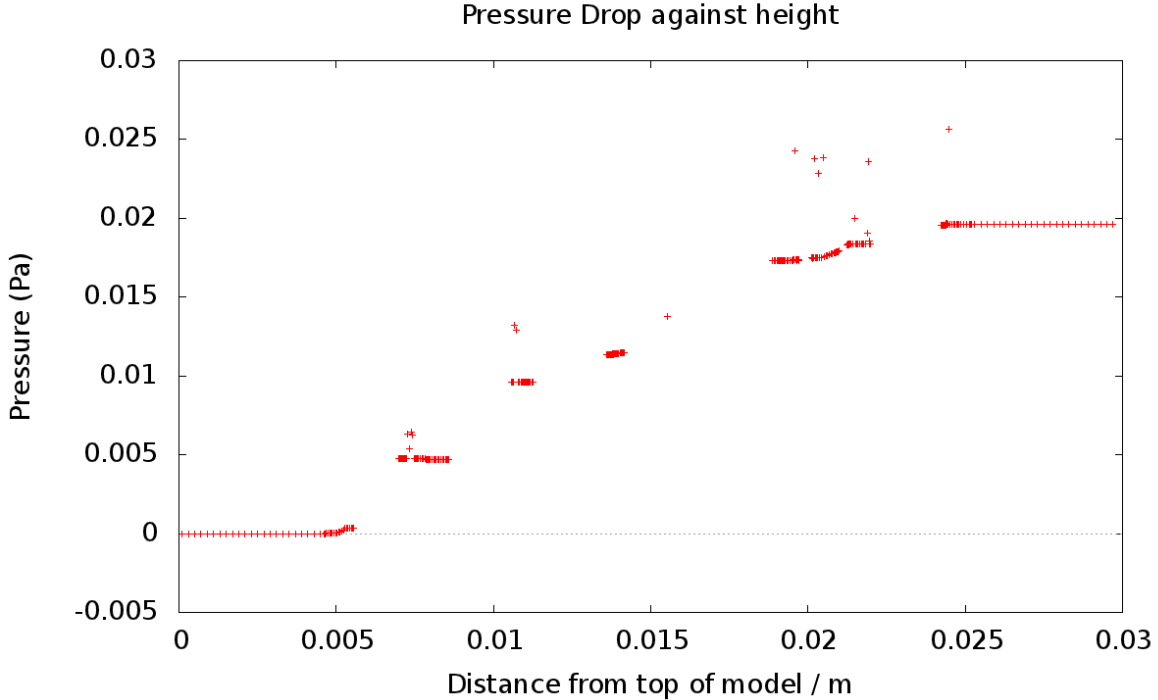


Figure 5.4: Graph of pressure against distance from base of model

$$K = \frac{0.0213 \times 0.1 \times \frac{12.75}{99} \times 1000 \times 9.8}{1.4}$$

$$K = 1.92 \text{m/s} \quad (5.3)$$

$$K = \frac{0.00284 \times 0.1 \times \frac{12.75}{99} \times 1000 \times 9.8}{0.101}$$

$$K = 3.55 \text{m/s} \quad (5.4)$$

The results from the models with a velocity of  $3.5 \times 10^{-4} \text{m/s}$  and  $2.84 \times 10^{-3} \text{m/s}$  gave a hydraulic conductivities value that were under  $0.1 \text{m/s}$  different to each other which suggests that these velocity values lie in the range for which Darcy's law is valid. This means that the hydraulic conductivity value for the sample of filter media that was taken from the case study is  $3.5 \text{m/s}$  according to this model. Both values of hydraulic conductivity were supplied to S. Winston-Gore[4] to enable the full model to be run using *SWMM5* and to compare the effect of the different values of hydraulic conductivity on a wider scale.

Comparing the value of hydraulic conductivity found by computational methods to the value found in the work by L. Whitehurst[22] served to finally validate the model. Although, due to discrepancies in the results from section 5.1, it was not expected that the two values would match. The value of hydraulic conductivity found experimentally in these permeameter tests was three orders of magnitude lower than the value obtained computationally.

For the CFD model to match up with the experimental data, the pressure drop would have to be three orders of magnitude greater due to hydraulic conductivity being calcu-

## CHAPTER 5: RESULTS

lated with equation 3.5. This shows that the CFD model is significantly under predicting the pressure drop. This could be attributed to multiple reasons. One possibility is that the small particles which were not able to be resolved by the micro-CT scanner combined with the smoothing during IBM has caused a significant change in the geometry. This can be validated due to the work by S. Pavey[2] where it was discovered that a small change in average particle diameter can have a significant change in the resultant pressure drop.

In section 5.1 the pressure drop from the CFD was an order of magnitude greater than the pressure drop from the experimental model. This is interesting as in this case the pressure drop from the CFD is three orders of magnitude less than the experimental data. Since as the experimental model used in section 5.1 was subject to the same loss of resolution as the CFD model described in above and the experimental method of calculating hydraulic conductivity was on the actual filter media so was not subject to any of these geometrical losses, there may be two causes of inaccuracy which need to be solved. Firstly potential errors caused during the modelling & IBM process, and those in the setup of the CFD model causing the error in section 5.1.

The hydraulic conductivity was also calculated for the media sample that was supplied directly from *Hydro International (UK)*. From the results in section 5.3 where it can be seen that the average grain size is significantly larger for this media sample than for the media sample taken from the case study, it would be expected that the hydraulic conductivity would be larger. For this model, the superficial velocity was  $3.5 \times 10^{-4}$  over a length of filter media of 0.016983, the results from this are calculated in equation 5.5.

$$K = \frac{0.00035 \times 0.016983 \times 1000 \times 9.8}{0.00262}$$

$$K = 22.2 \text{m/s} \quad (5.5)$$

As was expected the hydraulic conductivity value calculated for this sample is significantly larger, though due to the magnitude of the pressure drop not being considered to be accurate this is only an indication of the increased hydraulic conductivity on the sample of filter media that was obtained from *Hydro International (UK)* when compared to that which was found in the *Hydro Filterra™* unit of the case study.

It was discovered by J. Please[3] that it was possible to estimate the hydraulic conductivity of the filter media based on data from the sieve testing using relationships developed by Hazen[23]. While the values from this method are usually not used due to the variation in constants used which cause large deviations in the resultant hydraulic conductivities[24], a comparison between the values for the different filter media samples produced an interesting result.

J. Please[3] calculated the hydraulic conductivity for the filter media supplied by *Hydro International (UK)* to be  $1.089 \times 10^{-2} \text{m/s}$  while it was  $1.74 \times 10^{-3} \text{m/s}$  for the case study. As discussed above this is 6.26 times greater for the supplied filter media than the case study. As discussed above the values from the CFD are too large, although by comparing the values between the two samples it was possible to determine that the model was accurately representing the flow patterns. Comparison between the calculated hydraulic conductivity values for the two different sample sources obtained using CFD, produced a result showing that the value for the filter media supplied by *Hydro International (UK)* was 6.34 times the value from the case study. As proportions of the results from the CFD and from the work conducted by J. Please[3] are the same to two significant

figures it further suggests that the CFD model is accurately modelling the flow patterns through the filter media just with an incorrect magnitude which is potentially due to lack of a turbulence model.

## 5.5 Computational Time

The time taken to generate the meshes was not quantitative since *ScanIP* not have an inbuilt timer. To generate the meshes used in the improved and experimental models with large numbers of cells, approximately four hours was required.

The improved model run on the sample of filter media taken from the case study, needed the 12 core computer took on average 156 seconds per iteration, while the experimental model run on the 4 core Intel i7, took on average 244 seconds per iteration. Due to these large times per iteration the models took a significant period of time to complete the calculation, and this time doesn't include the time spent running the initial pressure calculations, splitting the model up for multi thread calculations and recombining the model after the simulation, each of which also took a significant amount of time.

## CHAPTER 6

# Conclusion

This project achieved all of the required deliverables on time as well as meeting the aims that were set at the start:

1. Create meshes for each media from the micro-CT data provided by the experimental team
2. Run CFD analysis on each mesh to identify relevant flow parameters under a range of flow conditions

The project went beyond its initial aims by comparing the results with experimental data of the same model in an attempt to validate the CFD, though it was this extension that proved that current model is not representative of the flow behaviour found in the experimental trials.

While overall the project has not been successful at producing a representative computational model of the filter media for *Hydro International (UK)*'s *Hydro Filterra™* system, it has not been a failure as it has shown that it is possible to create multiple computational models which follow the same trends as experimental data. There is scope for further work to be completed to accurately replicate like for like results.

This project has shown that it is possible to generate very detailed meshes based on actual pore geometries for computational fluid dynamics by using IBM and micro CT scanning which has never been achieved before on this scale. It has highlighted computational limitations as the entire project utilised machines at their computational limits. To enable progression involving the generation of more detailed meshes, access is needed to computers with significantly more RAM, as to generate the meshes used in this report 16GB of RAM and 30GB of swap was regularly required. A small increase in resolution at this scale has a significant effect on the amount of memory required. This is significant as it has been shown that a small change in the geometry can have a large effect on results at this scale.

Further work from this project would involve refining the mesh due to reduce the quantity of non-orthogonal and skewed cells in the mesh which are a possible cause of error. There is also scope for work to be done on investigating to what extent turbulence models are required. It could also be investigated if there are transient effects in the model which effect the drop in pressure over the filter media.

## CHAPTER 7

# References

- [1] Hydro International's image of the Hydro Filterra System <http://www.hydro-international.biz/images/pages/filterra-interactive.jpg>.
- [2] S. Pavey. Macro scale computational analysis including porous media and free surface interaction. 2012.
- [3] J. Please. please. 2012.
- [4] S. Winston-Gore. Investigating the wide scale impact of integrating a hydro filterra bioretention system within an urban drainage network using computational models. 2012.
- [5] M.J. Baker, P.G. Young, and G.R. Tabor. Image based meshing of packed beds of cylinders at low aspect ratios using 3d mri coupled with computational fluid dynamics. *Computers & Chemical Engineering*, 35(10):1969 – 1977, 2011.
- [6] Ziolkowska and Ziolkowski. Fluid flow inside packed beds. *Chemical Engineering and Processing: Process Intensification*, 23(3):137 – 164, 1988.
- [7] B Eisfeld and K Schnitzlein. The influence of confining walls on the pressure drop in packed beds. *Chemical Engineering Science*, 56(14):4321 – 4329, 2001.
- [8] P. C. Carman. Fluid flow through granular beds. *Transactions of the Institution of Chemical Engineers*, 15:150–166, 1937.
- [9] G.A. Narsilio, O. Buzzi, S. Fityus, T.S. Yun, and D.W. Smith. Upscaling of navier–stokes equations in porous media: Theoretical, numerical and experimental approach. *Computers and Geotechnics*, 36(7):1200–1206, 2009.
- [10] F.A.L. Dullien. *Porous media: fluid transport and pore structure*, volume 26. Academic press, 1992.
- [11] J. Bear. *Dynamics of fluids in porous media*. Dover publications, 1988.
- [12] P.G. Nutting. Physical analysis of oil sands. *Assoc. Petroleum Geologists Bull*, 14:1337–1349, 1930.
- [13] D. Ulrich, B. van Rietbergen, H. Weinans, and P. R̄egsegger. Finite element analysis of trabecular bone structure: a comparison of image-based meshing techniques. *Journal of Biomechanics*, 31(12):1187 – 1192, 1998.

## CHAPTER 7: REFERENCES

- [14] E.A.C. Johnson and P.G. Young. On the use of a patient-specific rapid-prototyped model to simulate the response of the human head to impact and comparison with analytical and finite element models. *Journal of Biomechanics*, 38(1):39 – 45, 2005.
- [15] CFD Online Wiki <http://www.cfd-online.com/>.
- [16] M Tierney, A Nasr, and G Quarini. The use of proprietary computational fluid dynamics codes for flows in annular packed beds. *Separation and Purification Technology*, 13(2):97 – 107, 1998.
- [17] Prashant R. Gunjal, Vivek V. Ranade, and Raghunath V. Chaudhari. Computational study of a single-phase flow in packed beds of spheres. *AICHE Journal*, 51(2):365–378, 2005.
- [18] M.J. Baker and G.R. Tabor. Computational analysis of transitional air flow through packed columns of spheres using the finite volume technique. *Computers & Chemical Engineering*, 34(6):878 – 885, 2010.
- [19] Jan and Tobis. Influence of bed geometry on its frictional resistance under turbulent flow conditions. *Chemical Engineering Science*, 55(22):5359 – 5366, 2000.
- [20] F R Menter. Two-equation eddy-viscosity turbulence models for engineering applications. *AIAA Journal*, 32(8):1598–1605, 1994.
- [21] MetOffice Regional mapped climate averages <http://www.metoffice.gov.uk/climate/uk/averages/regmapavge.html#wales>.
- [22] L. Whitehurst. Macro scale experimental investigation to determine the hydraulic properties of the hydro filterra bioretention system with comparison to the hydraulic performance of the case study. 2012.
- [23] A. Hazen. Disccusion: Dams on sand foundations. *Transactions of the American Society of Civil Engineers*, 73:199, 1911.
- [24] Alicia M. Wilson, Markus Huettel, and Stephen Klein. Grain size and depositional environment as predictors of permeability in coastal marine sands. *Estuarine, Coastal and Shelf Science*, 80(1):193 – 199, 2008.

## CHAPTER 8

# Appendix

## 8.1 Appendix A: List of Figures

1.1	<i>Hydro Filterra</i> <sup>TM</sup> system[1] . . . . .	2
2.1	Flow chart of the project . . . . .	6
2.2	Gantt chart of the project . . . . .	7
3.1	Similarity between a sample of stones and a packed bed . . . . .	8
3.2	Finite element (FE) model of the femoral head specimen[13] . . . . .	10
4.1	Sample of filter material taken from an active <i>Hydro Filterra</i> <sup>TM</sup> site . . .	16
4.2	Selection of filter media in <i>ScanIP</i> . . . . .	17
4.3	Selection of filter media in ScanIP in 3D . . . . .	18
4.4	Selection of flow in <i>ScanIP</i> . . . . .	18
4.5	Results for the initial model . . . . .	20
4.6	Selection of flow in <i>ScanIP</i> . . . . .	20
4.7	Results for the improved model . . . . .	21
4.8	Graph of the residuals . . . . .	23
4.9	Showing the part of the model that was created using ALM . . . . .	25
4.10	Pressure drop plotted against number of iterations to show convergence .	26
5.1	Comparison of P/l against Reynolds number for microCFD, macroCFD and experimental data . . . . .	27
5.2	CFD Results from the filter media taken from the case study . . . . .	29
5.3	CFD Results from the filter media supplied by Hydro . . . . .	30
5.4	Graph of pressure against distance from base of model . . . . .	31